Available online at www.sciencedirect.com
SCIENCE DIRECT
Polymer 46 (2005) 1077–1086
polymer
www.elsevier.com/locate/polymer

Composite magnetic particles: 1. Deposition of magnetite by heterocoagulation method

A. Pich*, S. Bhattacharya, H.-J.P. Adler

Institute of Macromolecular Chemistry and Textile Chemistry, Dresden University of Technology, D-01062 Dresden, Germany

Available online 8 December 2004

Abstract

In this paper we report synthesis and characterization of composite polymeric particles bearing magnetite inclusions and reactive β-diketone groups on the surface. Composites were prepared by two-step method in which first step requires preparation of the functionalized polystyrene core and during second step magnetite was deposited onto core particle surface. This procedure gives a possibility to obtain composite particles with core-shell morphology and both the core size and magnetite shell thickness can be varied. Highly monodisperse PS/AAEM microspheres were synthesized by surfactant-free emulsion polymerization. Change of monomer fleet-ratio gives a possibility to change effectively the final particle size of dispersions without strong changes in particle size distribution. PS/AAEM particles were characterized by light scattering techniques (DLS, SLS) and electron microscopy (SEM) with respect to their particle size and morphology of the surface layer. Magnetite was deposited in form of nano-crystals onto PS-AAEM particle surface by heterocoagulation process. It has been established that more uniform magnetite coating was obtained at lower base amounts used for synthesis of magnetite. Amount of the magnetite on the polymeric particle surface can be effectively controlled by changing the initial $FeCl_2$ and $FeCl_3$ concentrations and/or variation of the PS/AAEM core dimensions. It has been confirmed by separation centrifugation technique, that stepwise increase of the magnetite content on the particle surface decrease gradually the stability of colloidal system. Magnetization curves for composite particles indicate that deposited magnetite content is high enough to achieve considerable magnetic response to external magnetic field.

Keywords: Latex particles; Core-shell; Magnetite

1. Introduction

Nano-coating techniques lead to the formation of novel inorganic–organic functional hybrid materials with tailored properties that depend on the combination of components employed in the fabrication process. Materials for specific applications in catalysis, electronics, biomaterials engineering can be designed by careful selection of the components and template morphology. The majority of the templates used for preparation of hybrid materials can be produced at the present moment with monodisperse size (colloid particles) or of controlled morphology (membrane pore structure, cross-linking density of gel etc.).

There is a considerable interest in preparation of magnetite (Fe_3O_4) due to its strong magnetic properties, which were used first in biology and then in medicine for the magnetic separation of biochemical products [1] and cells [2] as well as the magnetic guidance of particle systems for site-specific drug delivery [3]. However, the size, charge, and surface chemistry of magnetic particles could strongly influence their magnetic properties [4] and distribution in biological systems [5–7]. The most common method for the synthesis of magnetite is by co-precipitation from a solution of Fe(III) and Fe(II) salts in presence of base [8–11]. Preparation of size-controllable magnetite nano-particles was performed in presence of different water-soluble polymers such as lignosulfonate [12], mesoporous sulfonated styrene-divinylbenzene [13], polypeptide [14] etc. Magnetite nano-particles have been also incorporated into more complicated architectures, such as polymeric gels providing formation of magnetic field sensitive gels [15,16]. These gels contain magnetic particles dispersed homogeneously and confined in a polymer network. Under a non-uniform magnetic field, the particles undergo motion, which

* Corresponding author. Tel.: +49 351 463 33782; fax: +49 351 463 37122.
E-mail address: andrij.pich@chemie.tu-dresden.de (A. Pich).

0032-3861/$ - see front matter © 2004 Elsevier Ltd. All rights reserved.
doi:10.1016/j.polymer.2004.11.043

in turn induces elongation, contraction, or bending of the gels with short response time. Incorporation of magnetite into spherical polymeric particles has been achieved by following two approaches: (1) heterocoagulation of magnetite on the surface of pre-formed polymeric particles [17,18], (2) encapsulation of magnetite particles during emulsion polymerization process [19–22] or by using the microemulsion approach [23–27], or (3) by layer-by-layer deposition method [28,29].

The motivation for this study was preparation of non-porous polymeric microspheres with large external surface area and reactive surface for enzyme immobilization. The size of such microspheres should be considerably reduced to achieve large surface area, therefore solid–liquid separation process becomes more demanding. From this point of view incorporation of magnetite into polymeric particles can solve the separation problem. Present paper is the first in series explaining the preparation of monodisperse latex particles functionalized with β-diketone groups. In present study we used probably the most direct and versatile approach for the modification of the latex particle surface when a functional monomer is used directly in one-step copolymerization process. Due to the intrinsic interfacial activity of functional monomer it spontaneously migrates and accumulates on the particle surface leading to formation of highly reactive surface. Since β-diketone groups are capable to chelate effectively metal ions and react with amino groups, so the high efficiency for magnetite loading and enzyme immobilization can be expected. Investigations were performed in two directions: (a) preparation of magnetite in presence of functionaized polymeric particles and (b) encapsulation of pre-formed magnetite particles during heterophase polymerization process. This paper summarises the results about formation of magnetite in presence of functionalized microspheres which leads to the formation of core-shell type particles.

2. Experimental part

2.1. Materials

Styrene (ST) (from Fluka) and acetoacetoxyethyl methacrylate (97%) (AAEM) (from Aldrich) were purified by vacuum distillation. Sodium peroxydisulfate (97%) (SPDS) and 2,2′-azobis(2-methylpropyonamidine) dihydrochloride (97%) (AMPA), iron (III) chloride ($FeCl_3$), and iron (II) chloride ($FeCl_2$) were received from Aldrich and used as commercially available. Ammonium hydroxide (NH_4OH) in form of 40% water solution was obtained from Fluka. Distilled water was employed as polymerization medium.

2.2. Synthesis of PS/AAEM core particles

Double-wall glass reactor equipped with stirrer and reflux condenser was purged with nitrogen. Water (170 g) and appropriate amounts of ST (19 g) and AAEM (1 g, 5% to ST) were added into reactor and stirred at room temperature. After 10 min temperature was increased to 70 °C and water solution of initiator (0.3 g SPDS in 10 g water) was added to start the polymerization process. Latexes were prepared at ca. 10% solid content.

2.3. Synthesis of composite particles

Preparation of magnetite was performed according to modified method described in Ref. [11]. Diluted PS/AAEM dispersions were placed into stirred reactor and mixture was stirred for 15 min under nitrogen flow at 25 °C. Solutions of $FeCl_2$ and $FeCl_3$ were prepared in separate flasks and added to stirred dispersion under nitrogen blanket (molar ratio $FeCl_3/FeCl_2$ was kept constant at 2:1). Water solution of NH_4OH was added drop-wise to start magnetite formation process. Immediately after base addition dispersion became dark-brown indicating that magnetite has been formed in the system. After 30 min formed composite particles were removed from reaction vessel and cleaned by precipitation to remove all by-products.

2.4. Analytical methods

2.4.1. Particle size analysis

A commercial laser light scattering (LLS) spectrometer (ALV/DLS/SLS-5000) equipped with an ALV-5000/EPP multiple digital time correlator and laser goniometer system ALV/CGS-8F S/N 025 was used with a helium–neon laser (Uniphase 1145P, output power of 22 mW and wavelength of 632.8 nm) as the light source. With static LLS it is possible to obtain both the weight–average molar mass (M_w) and the z-average radius of gyration R_g of scattering objects in an extremely dilute solution because Rayleigh ratio $R(q)$, is dependent on the scattering vector q as:

$$\frac{Kc}{R(q)} = \frac{1}{M_w}\left(1 + \frac{(qR_g)^2}{3}\right) + 2A_2c \tag{1}$$

where

$$K = 4\pi^2 n^2 (\mathrm{d}n/\mathrm{d}c)^2/(N_A\lambda_0^4) \tag{2}$$

$$q = (4\pi n\lambda_0)\sin(\theta/2) \tag{3}$$

with n, c, N_A, λ_0 with θ being the solvent refractive index, sample concentration, the Avogadro's number, the wavelength of the incident light in a vacuum, the scattering angle and concentration, respectively.

In dynamic LLS, the intensity–intensity–time correlation function $g_2(q,t)$ in the self-beating mode was measured and can be expressed by the Siegert relation:

$$g_2(q,t) = A(1 + \beta|g_1(q,t)|^2) \tag{4}$$

where t is the decay time, A is a measured baseline, β is the

coherence factor, and $g_1(q,t)$ is the normalized first-order electric field time correlation function and $g_1(q,t)$ is related to the measured relaxation rate Γ:

$$g_1(q,t) = \int G(\Gamma)\exp(-\Gamma t)\mathrm{d}\Gamma \quad (5)$$

A line-width distribution $G(\Gamma)$ can be obtained from the Laplace inversion of $g_1(t)$ (CONTIN procedure) [10]. For a pure diffusive relaxation, Γ is related to the translational diffusion coefficient D at $q \to 0$ and $c \to 0$ by

$$D = \Gamma/q^2 \quad (6)$$

or a hydrodynamic radius R_h given by

$$R_h = k_B T/(6\pi\eta D) \quad (7)$$

with q, k_B, T and η being scattering vector, the Boltzman constant, absolute temperature, and solvent viscosity, respectively. All DLS experiments were carried out at angles $\theta = 30$–$140°$. The sample in a 10 mm test tube was immersed in a toluene bath and thermostated within an error of ± 0.1 °C. Typically, three measurements were performed for determination of the radius of gyration and five for the hydrodynamic radius. Accuracy of measurements for radius of gyration is $\pm 6\%$, for hydrodynamic radius is $\pm 3\%$.

2.4.2. Stability measurements

Stability measurements were performed with separation analyser LUMiFuge 114 (L.U.M. GmbH, Germany). Measurements were made in glass tubes at acceleration velocities from 500 to 3000 rpm. The slope of sedimentation curves was used to calculate the sedimentation velocity and to get information about stability of the samples.

2.4.3. Scanning electron microscopy (SEM)

SEM images were taken with Gemini microscope (Zeiss, Germany). Samples were prepared in the following manner. Dispersions were diluted with deionized water, dropped onto aluminium support and dried at room temperature. Samples were coated with thin Pd layer to increase the contrast and quality of the images. Pictures were taken at voltage of 4 kV.

2.4.4. IR-Spectroscopy

IR spectra were recorded with Mattson Instruments Research Series 1 FTIR spectrometer. Dried polymer samples were mixed with KBr and pressed to form a tablet.

2.4.5. Thermo gravimetrical analysis (TGA)

To determine the magnetite content in composite particles the TGA 7 Perkin–Elmer instrument (Pyris-Software Version 3.51) was used. Before measurement samples were dried in vacuum for ca. 48 h. Samples were analyzed in closed aluminium cups in temperature range 25–600 °C (heating rate 5 K/min in nitrogen atmosphere).

2.4.6. Magnetization measurements

The vibrating-sample magnetometer (VSM Oxford) was used to study the magnetic properties of composite particles with a maximum magnetic field of 1 T at 290 K.

3. Results and discussion

3.1. Preparation of PS/AAEM particles

PS/AAEM particles have been prepared by surfactant-free co-polymerization of styrene and acetoacetoxyethyl methacrylate (AAEM). Due to the hydrophilic character of AAEM it can provide some sterical stabilization to formed particles. It can be also assumed that the surface layer of PS/AAEM particles will consist mostly out of AAEM-rich polymer chains and core region will be occupied by more hydrophobic polystyrene. Fig. 1 shows that the size of PS/AAEM particles measured by DLS can be effectively varied by fleet-ratio (W_{AAEM}/W_{ST}) or the macroscopic weight ratio of both monomers. It is clear from Fig. 1 that formed polymeric particles are of sub-micrometer size and gradual increase of AAEM in the system leads to smaller particle dimensions because in this way larger surface area can be effectively protected. It is also obvious that increase of acrylate amount in reaction mixture makes the changes of hydrodynamic radii less pronounced and finally at high AAEM contents R_h becomes nearly not influenced by initial monomer composition.

Obtained particles had narrow particle size distribution. Detailed investigations were performed by using combination of dynamic and static light scattering together with electron microscopy. Fig. 2 shows the comparison of particle size measurements obtained from different analytical techniques.

Obtained results confirm that the particle size of PS/AAEM particles decreases when AAEM content is higher. It is also obvious that the agreement between different analytical techniques is very good. It should be noted that results shown in Fig. 2 are hydrodynamic radii

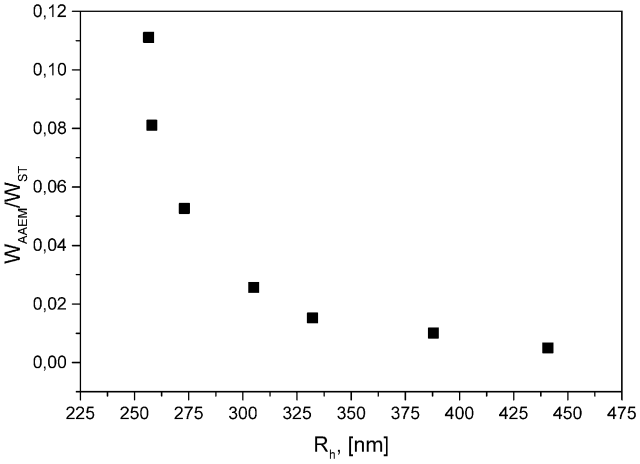

Fig. 1. Fleet-ratio (W_{AAEM}/W_{ST}) of monomers used in polymerization plotted vs hydrodynamic radii (R_h) of the final PS/AAEM particles.

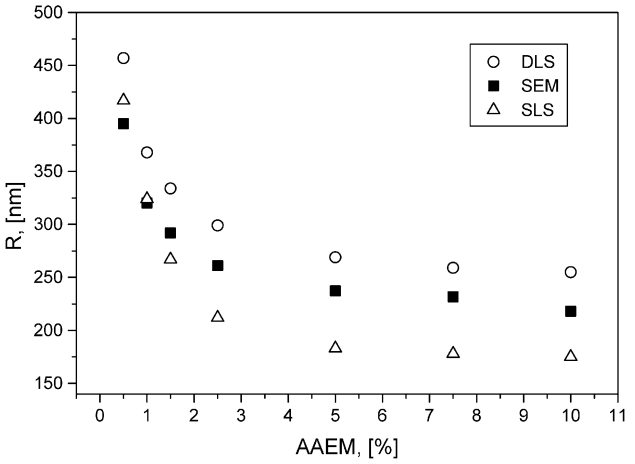

Fig. 2. Particle radii of the PS/AAEM spheres as a function of AAEM content.

(R_h) measured by means of DLS, radius of gyration (R_g) measured by SLS and 'hard core' radius (R) obtained from SEM. Experimental result from Fig. 2 have been used to calculate hydrodynamic shell thickness (ΔR) and R_g/R_h ratio (or ρ-parameter). When we consider that particle surface in water solution is in swollen state then the difference between R_h and R should provide information about hydrodynamic shell thickness (ΔR) (see Fig. 3(1)). The R_g/R_h ratio provides useful information about the particle shape and can be compared to theoretical value for sphere (see Fig. 3(2)).

It is obvious from Fig. 3(1) that the hydrodynamic shell thickness decreases gradually if the AAEM content increases. The explanation for this effect is probably increase of particle number and the total surface area in the system with increasing AAEM content. So, for smaller particles AAEM-rich layer will be thinner because it has to be 'distributed' on larger amount of particles. Calculated R_g/R_h values for different particles show similar tendency—initial decrease up to certain acrylate content and then more or less constant data for particles containing larger AAEM amounts. The dotted line in Fig. 3(1) indicates the theoretical value for spherical particles $R_g/R_h = 0.774$. Calculated R_g/R_h values do not fit exactly to the theoretical value, but considerable correlation can be observed (at least for particles with higher AAEM content). SEM images shown in Fig. 4 indicates that obtained particles possess spherical shape and in agreement with light scattering results smaller particles have been formed at higher AAEM content.

The incorporation of AAEM into particles was confirmed by IR-spectroscopy. Fig. 5 shows IR spectra of PS/AAEM particles prepared with different acrylate amounts. Characteristic signal at ca. 1750 cm^{-1} (peaks marked with arrows in Fig. 5) corresponds to C=O vibration mode. It is clear that the intensity of this signal increases gradually, if AAEM content in composite particles is higher. At the same time the intensity of typical PS signals at 1450 and 1500 cm^{-1} remain constant.

The stability of PS/AAM particles was investigated by sedimentation method developed by Lerche et al. [30]. In special centrifuge an integrated optoelectronic sensor system allows spatial and temporal changes of light transmission during the rotation to be detected. In contrast to other approaches [31] the local transmission is determined over the entire sample length simultaneously. Throughout the measurement, transmission profiles are recorded and sedimentation process can be depicted as a time course of the relative position of the boundary between supernatant and sediment (resolution better than 100 μm) or of the transmission averaged over the entire or a chosen part of the sample length. On the basis of obtained data the sedimentation constants, the packing density, etc. can be derived.

The transmission profile of sedimentation process for PS/AAEM sample containing 10% AAEM in Fig. 6 shows

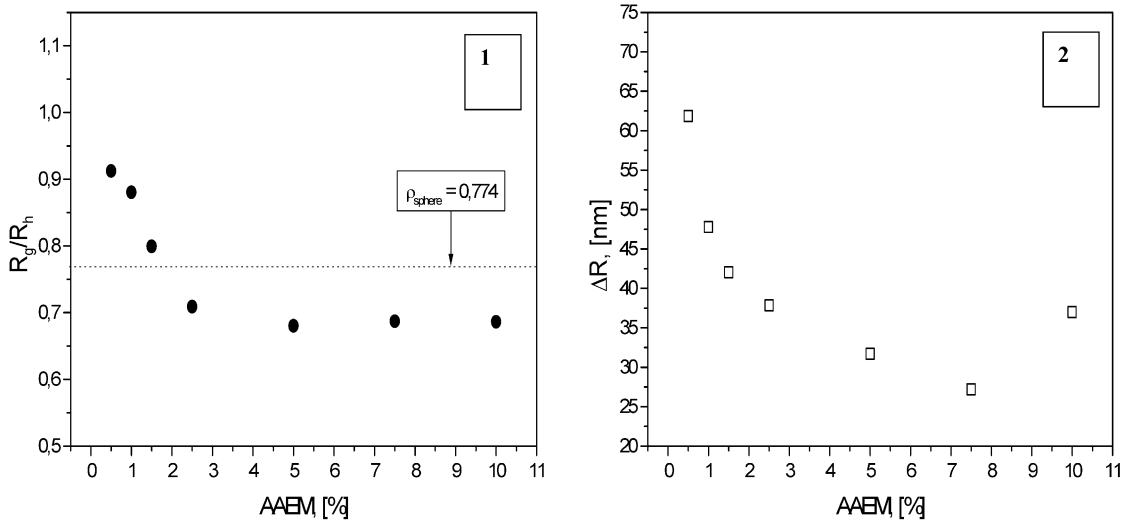

Fig. 3. Variation of R_g/R_h ratio (1) and hydrodynamic shell thickness ΔR (2) for the PS/AAEM particles with AAEM content.

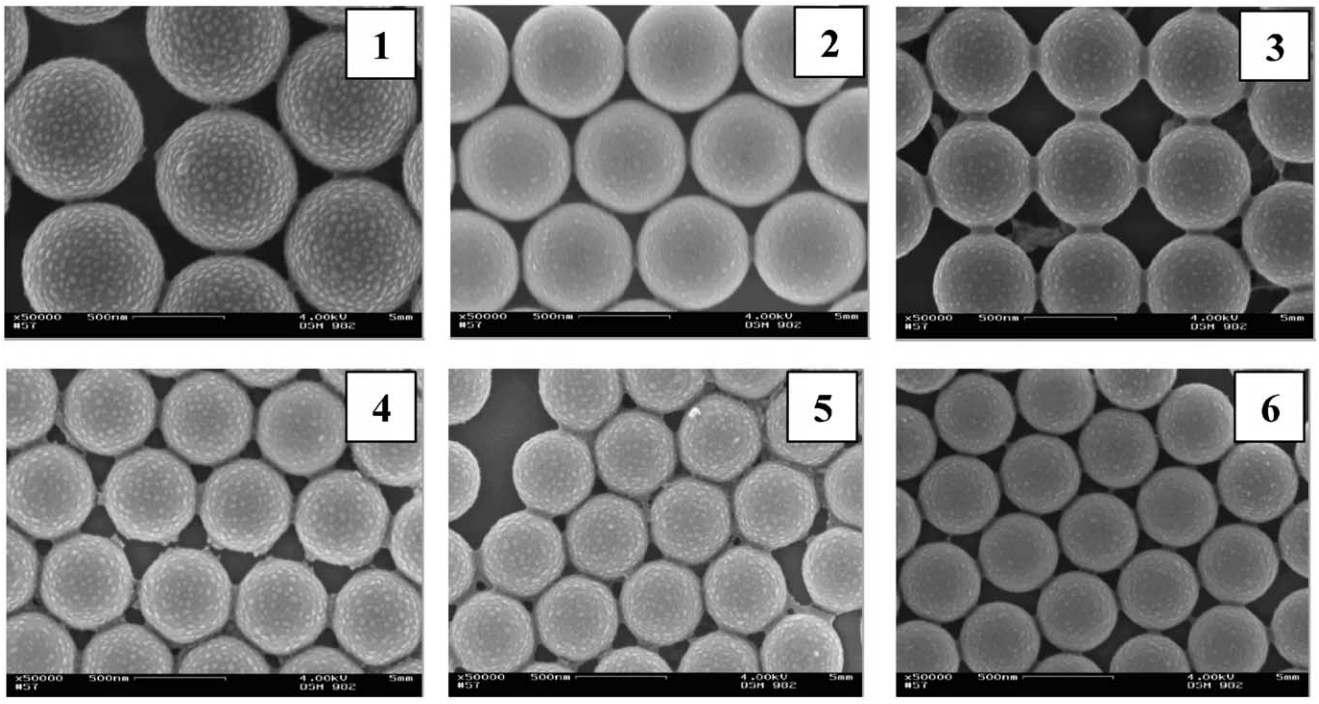

Fig. 4. SEM images of PS-AAEM particles prepared at different AAEM contents (1–0.5%; 2–1%; 3–1.5%; 4–2.5%; 5–5%; and 6–7.5%).

continuous decrease in sediment height due to compression of the sediment. Fig. 6 shows that sedimentation front is moving to the bottom of cuvette and the light transmission increases. In this case the transmission profiles were recorded every 10 s and every 10th measurement is shown.

Fig. 6 shows that a sedimentation fronts move parallel to the cuvettes bottom indicating stepwise particle precipitation. The transmission profiles can be transformed into sedimentation–time curves (Fig. 7). These curves represent actually the demixing curves and the motion of the interphase between clear phase (water) and sediment toward the cuvette bottom as a function of time. Fig. 7 shows sedimentation–time curves measured at 3000 rpm for PS/AAEM particles prepared at different compositions. The difference in slope of the sedimentation curves indicate that particles which contain low AAEM amounts precipitate faster if to compare with particles containing more AAEM.

The calculated sedimentation rates from the slopes of sedimentation–time curves measured at different rotation velocities are summarized in Fig. 8.

The sedimentation rate increases with increasing rotation speed and particle size of dispersions (at lower AAEM contents larger particles have been obtained). Fig. 8 also indicates that sedimentation velocity data for particles prepared with 5, 7.5 and 10% AAEM are similar because the particle dimensions of above mentioned particles do not vary considerably (see Fig. 1). The sedimentation rate (v)

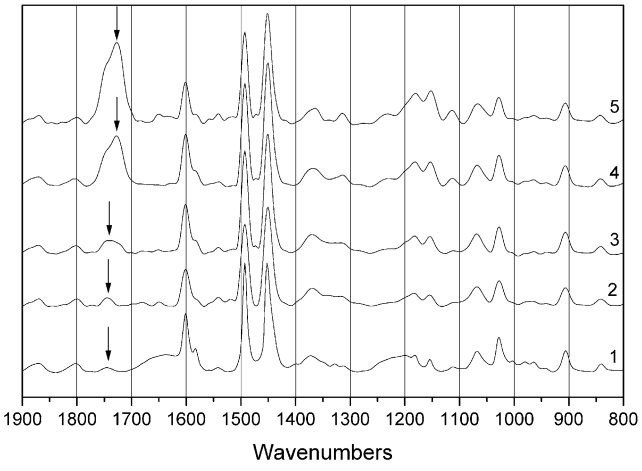

Fig. 5. IR spectra of PS/AAEM particles (2–0.5%; 3–1.5%; 4–5%; 5–10%; 1-PST reference).

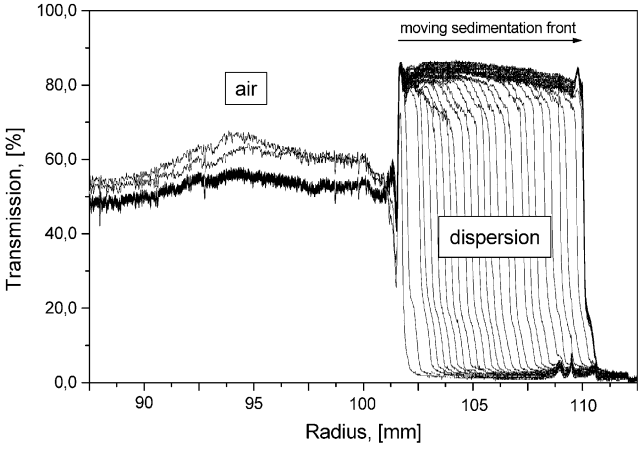

Fig. 6. Transmission profiles recorded during sedimentation process for PS/AAEM particles containing 10% AAEM (rotation speed—3000 rpm).

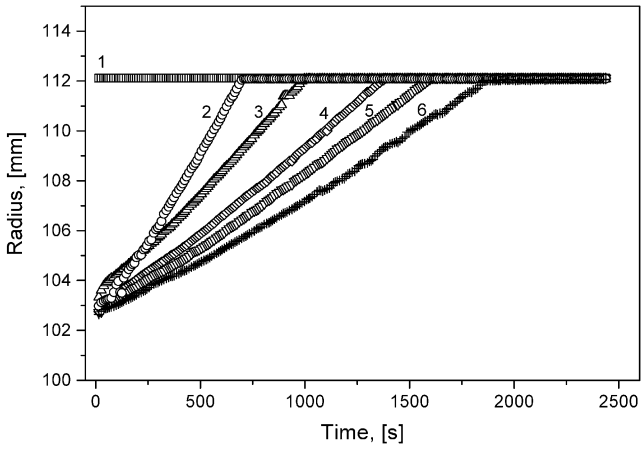

Fig. 7. Sedimentation curves for PS/AAEM particles with different AAEM content (1–water; 2–0.5%; 3–1%; 4–2.5%; 5–5%; 6–7.5%) at rotation speed 3000 rpm.

for particles in diluted system can be defined as:

$$v = \frac{2r^2\,\Delta\rho\,xg}{9\eta} \tag{8}$$

where r—is particle radius, $\Delta\rho$—is density difference, xg—is centrifugal acceleration and η—is the viscosity of medium. From Eq. (5) it is clear that the sedimentation velocity should increase if particle size, centrifugal force or density difference between particles and medium increase.

3.2. Deposition of magnetite

The formation of magnetite nano-particles was performed in presence of PS/AAEM latex to investigate the possibility of composite particle formation by hetero coagulation method. In this case several factors should influence strongly the magnetite deposition process and the morphology of composite particles. Since for magnetite formation is favored in basic medium, several reactions were performed to study the influence of added amount of NH_4OH on composite particle formation. In this reaction set pH value of reaction mixture was close to 10, but the base amount was gradually reduced.

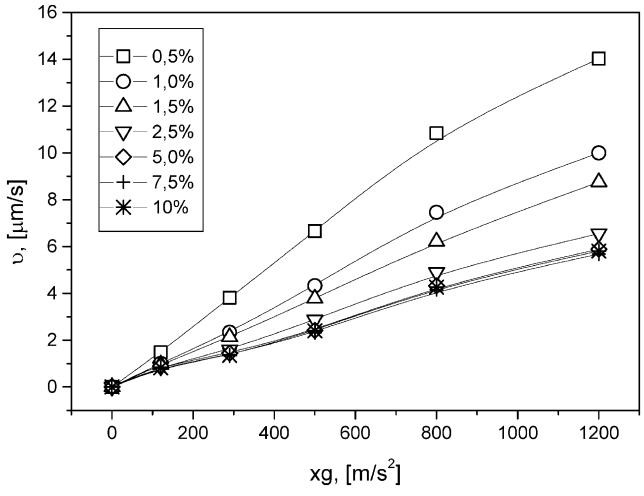

Fig. 8. Sedimentation velocity for PS/AAEM samples with different AAEM contents as a function of centrifugal acceleration.

SEM images of composite particles prepared at different base concentrations by using PS/AAM particles with 5% AAEM are shown in Fig. 9. Micrographs indicate clearly that if NH_4OH concentration in reaction mixture is reduced the coating of PS/AAEM particles becomes more uniform and less magnetite can be found beside polymeric cores. Probably at high excess of NH_4OH these molecules can stabilize partly newly formed magnetite particles and they prefer to stay in water solution and not to be adsorbed on PS/AAEM surface. It should be noted that reduction of base amount does not reduce the amount of produced magnetite, so in our next investigations base concentration in the system was fixed at 0.7 M.

In next experimental set PS/AAEM particles with 5% AAEM were coated with different magnetite amounts. Amount of the magnetite on the polymeric particle surface can be effectively controlled by changing the initial $FeCl_2$ and $FeCl_3$ concentrations. Table 1 shows the amounts of ingredients used for preparation of composite particles and deposited magnetite amount calculated from TGA measurements.

Obtained particles were characterized with respect to their magnetic properties. Magnetization curves for particles bearing different magnetite contents are shown in Fig. 10. The magnetic response to external field increases if the magnetite amount deposited onto PS/AAEM surface is rising up. This plot demonstrates that it is possible to control the magnetic properties of composite particles simply by influencing the deposition process.

Microscopy investigations have been performed to investigate the morphology of composite particles. Fig. 11 shows SEM images of PS/AAEM particles with different magnetite contents on the surface.

Microscopy images indicate that generally the amount of magnetite inclusions on the particle surface becomes larger; however, only at high magnetite loads the formation of more or less compact shell can be observed. At lower magnetite loads Fe_3O_4 inclusions are not really homogeneously distributed on PS/AAEM particle surface and sometimes form aggregates or clusters on core particle surface. In case of low magnetite load the ratio base: Fe_3O_4 is still high and

Table 1
Preparation of magnetic particles (in every run 10 g of PS/AAEM latex was diluted 40 g water and 10 g of 0.7 M NH_4OH was added)

Sample	$FeCl_2$ [g]	$FeCl_3$ [g]	Fe_3O_4 [%]
1	0.039	0.108	7.28
2	0.049	0.134	7.30
3	0.066	0.18	11.05
4	0.099	0.268	13.77
5	0.109	0.536	19.96

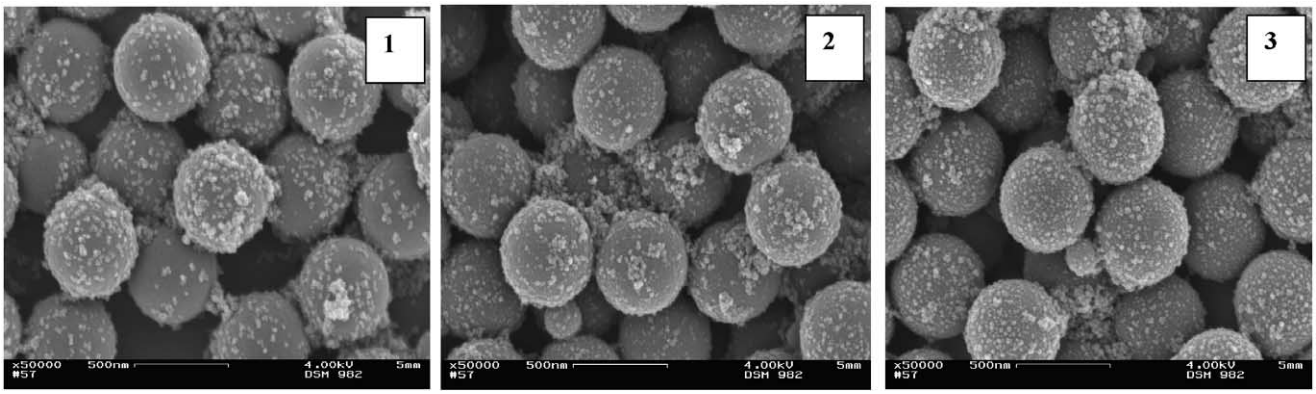

Fig. 9. Composite particles prepared at different concentrations of NH_4OH in the reaction mixture (1–7 M; 2–3.5 M; 3–0.7 M).

some inorganic particles can be stabilized in water phase and depleted from the polymer particle surface. Increase of magnetite load decreases base amount (respectively to amount of formed magnetite), so deposition on the particle surface becomes more favorable process.

The stability of composite particles was investigated in similar manner as for PS/AAEM particles to determine the influence of magnetite amount loaded on the particle surface on sedimentation velocity.

Fig. 12 shows that deposition of magnetite on PS/AAEM content decreases the stability of colloidal system. This effect can be explained by interaction of magnetite nanoparticles with AAEM-rich shell. This hydrophilic layer is responsible for sterical stabilization of particles providing sufficient repulsion forces between particles. Magnetite inclusions probably 'deactivate' this protective layer by adsorption or chelate formation with ketone groups of AAEM. It can be seen from Fig. 11 that if the deposited amount of magnetite is larger 10% the sedimentation speed increases dramatically indicating very poor stability of obtained composite particles.

In next reaction set equal magnetite amounts were deposited on PS/AAEM particles prepared with different AAEM contents. In this case the weight ratio between core and magnetite was kept constant, but since AAEM content influences strongly the particle size it can be expected that the surface area of latex template has been changed.

Magnetization curves shown in Fig. 13 indicate that obtained composite particles exhibit similar magnetic response since similar magnetite amounts were deposited in every case (good correlation with determined magnetite amounts presented in Table 2).

SEM images shown in Fig. 14 indicate that magnetite

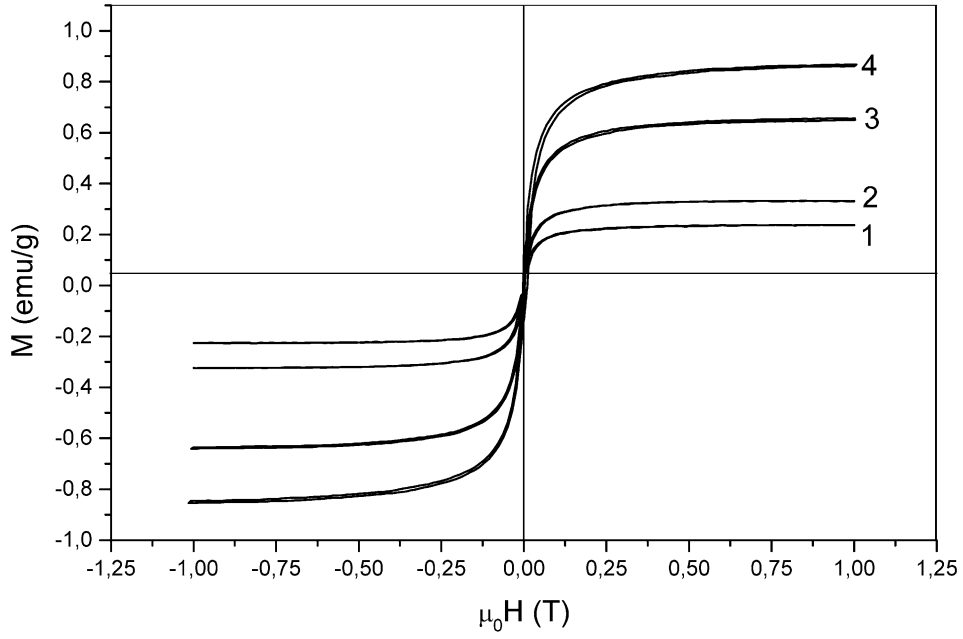

Fig. 10. Magnetization curves of composite particles with different magnetite contents as a function of applied magnetic field (1–7.28%; 2–7.30%; 3–11.05%; 4–13.77%).

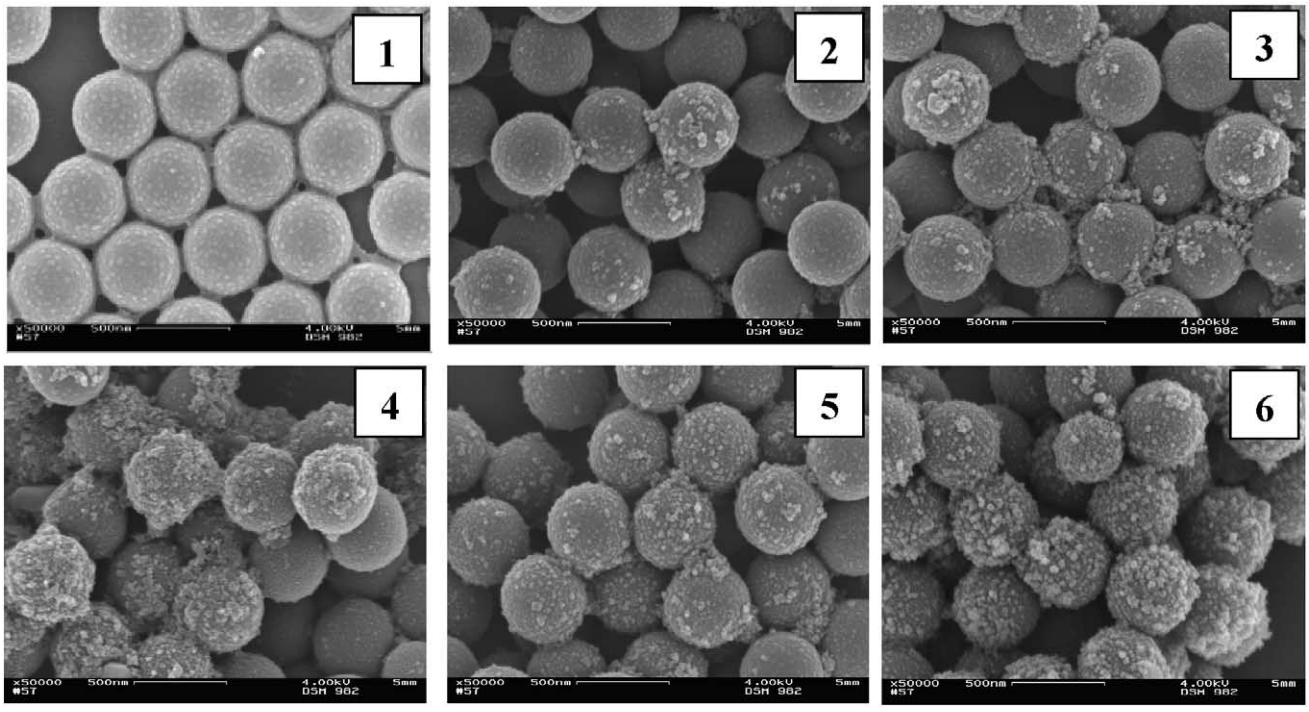

Fig. 11. SEM images of composite particles with different magnetite contents (1–core; 2–7.28%; 3–7.30%; 4–11.05%; 5–13.77%; 6–19.96%).

deposition on the surface of larger PS/AAEM spheres leads to more uniform composite particles, however, still some discrete magnetite particles can be found beside the composites.

It has been shown in Fig. 3(1) that at higher AAEM contents (smaller particles) the thickness of hydrodynamic shell decreases and probably AAEM unit's number per particle becomes smaller. Therefore, deposition of magnetite on the surface of smaller PS/AAEM particles is not really favorable. It seems that larger spheres can stabilize more effectively magnetite inclusions due to the optimal architecture of the surface layer.

4. Conclusions

In this study we investigated synthesis and properties of composite polymeric particles containing magnetite (Fe_3O_4). Obtained particles should combine two important features: (a) high response to external magnetic field, and

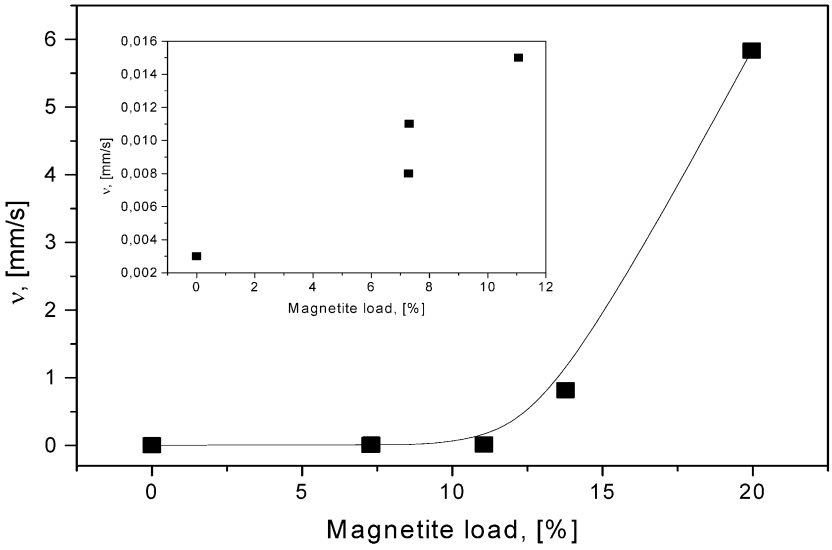

Fig. 12. Sedimentation velocity for PS/AAEM samples with different magnetite loads (inset shows the situation at lover magnetite contents) (rotation speed—3000 rpm).

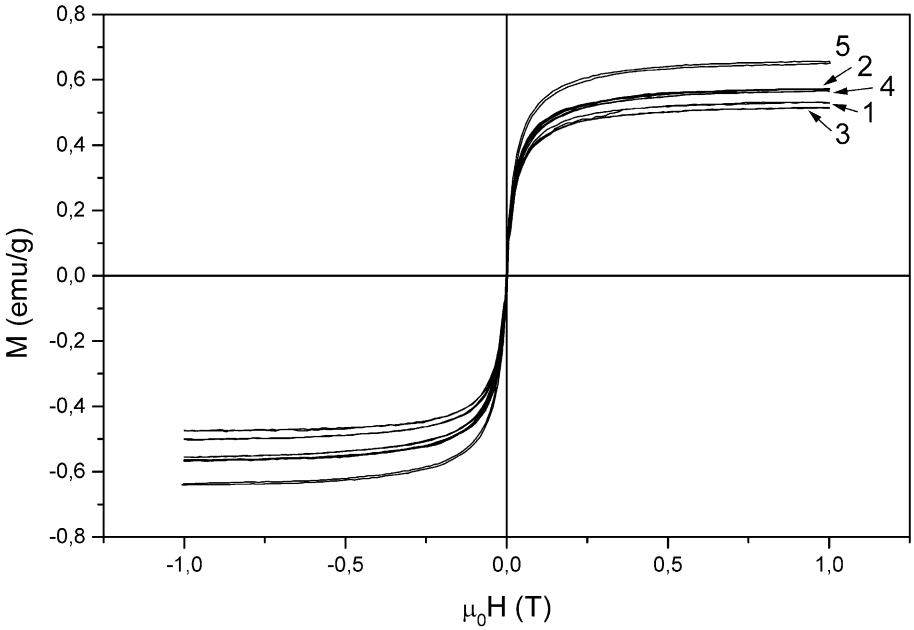

Fig. 13. Magnetization curves of composite particles with different core size as a function of applied magnetic field (1–457 nm; 2–368 nm 3–334 nm; 4–299 nm; 5–269 nm).

(b) functionalization of the particle surface with reactive groups capable to bind bio-molecules. Composites were prepared by two-step procedure, where magnetite nano-particles have been deposited onto the pre-formed polymeric cores providing formation of magnetic shell. Following approach highly monodisperse PS/AAEM microspheres were synthesized by surfactant-free emulsion polymerization. Change of monomer fleet-ratio gives a possibility to change effectively the final particle size of dispersions without strong changes in particle size distribution. PS/AAEM particles were characterized by light scattering techniques (DLS, SLS) and electron microscopy (SEM) with respect to their particle size and morphology of the surface layer. Magnetite was deposited onto PS/AAEM particle surface by heterocoagulation process of formed Fe_3O_4 nano-crystals. It has been established that more uniform magnetite coating was obtained at lower base amounts used for synthesis of magnetite. Amount of the magnetite on the polymeric particle surface can be effectively controlled by changing the initial $FeCl_2$ and $FeCl_3$ concentrations and/or variation of the PS-AAEM core dimensions. Loaded magnetite contents were determined by thermal gravimetrical analysis (TGA). It has been confirmed by means of separation analyser, that stepwise increase of the magnetite content on the particle surface decrease gradually the stability of colloidal system. Magnetization curves measured for composite particles indicate that deposited magnetite content is high enough to

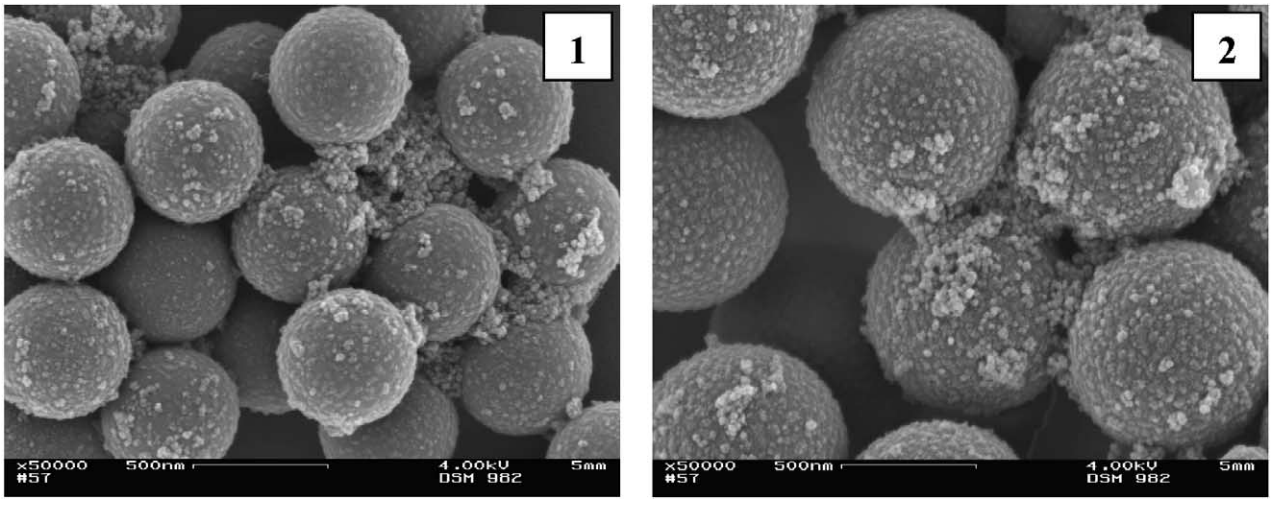

Fig. 14. SEM images of composite particles with different core radii (1–269 nm; 2–457 nm).

Table 2
Preparation of magnetic particles (in every run 10 g of PS/AAEM latex was diluted 40 g water and 10 g of 0.7 M NH_4OH was added)

Sample	R_h [nm]	$FeCl_2$ [g]	$FeCl_3$ [g]	Fe_3O_4 [%]
1	457	0.066	0.18	11.36
2	368	0.066	0.18	9.59
3	334	0.066	0.18	9.54
4	299	0.066	0.18	11.08
5	269	0.066	0.18	11.05

achieve considerable magnetic response to external magnetic field.

Acknowledgements

The authors are thankful to Mrs. E. Kern for SEM measurements, Deutsche Forschungsgemeinschaft (DFG) with collaboration research project SFB 287 'Reactive Polymers' for financial support.

References

[1] Patton WF, Kim J, Jacobson BS. Biochim Biophys Acta 1985;816:83.
[2] Kemshead JT, Treleaven JG, Gibson FM, Ugllstad J, Rembaum A, Philip T. Prog Exp Tumor Res 1985;29:249.
[3] Gupta PK, Hung CT. Life Sci 1989;44:175.
[4] Pouliquen D, Perroud H, Calza F, Jallet P, Le Leune JJ. Magn Reson Med 1992;24:75.
[5] Bengle HH, Palmacci S. Magn Reson Imaging 1994;12:433.
[6] Josefson L, Lewis J, Jacobs P, Hahn PF, Stark DD. Magn Reson Imaging 1988;6:647.
[7] Papisov MI, Bogdanov Jr A, Schaffer B, Nossiff N, Shen T, Weisleder R, Brady TJ. J Magn Magn Mater 1993;122:383.
[8] Shalafalla EK, Reimers GW. IEEE Trans Magn 1980;16:178.
[9] Massart R. IEEE Trans Magn 1981;17:1247.
[10] Sato T, Iijima T, Seki M, Inagaki N. J Magn Magn Mater 1987;65:252.
[11] Buske N, Sonntag H, Götze T. Colloids Surf 1984;12:195.
[12] Hassett KL, Stecher LC, Hendrickson DN. Inorg Chem 1980;19:416.
[13] Rabelo D, Lima ECD, Reis AC, Nunes WC, Novak MA, Garg VK, Oliveira AC, Morais PC. Nano Lett 2001;1:105.
[14] Tiefenauer LX, Kühne G, Andres RY. Bioconjugate Chem 1993;4:347.
[15] Narita T, Knaebel A, Munch JP, Candau SJ, Zrinyi M. Macromolecules 2003;36:2985.
[16] Chatterjee J, Haik Y, Chen CJ. Colloid Polym Sci 2003;281:892.
[17] Fang M, Grant PS, McShane M, Sukhorukov GB, Golub VO, Lvov YM. Langmuir 2002;18:6338.
[18] Lvov Y, Caruso F. Anal Chem 2001;73:4212.
[19] Xu X, Friedman G, Humfeld KD, Majetich S, Asher SA. Chem Mater 2002;14:1249.
[20] Chen JP, Su DR. Biotechnol Prog 2001;17:369.
[21] Horak D, Rittich B, Safar J, Spanova A, Lenfeld J, Benes MJ. Biotechnol Prog 2001;17:447.
[22] Gu S, Shiratori T, Konno M. Colloid Polym Sci 2003;281:1076.
[23] Mobe G, Kon-no K, Kyori K, Kitahara A. J Colloid Inerface Sci 1983;93:293.
[24] Lee KM, Corensen MS, Klabunde JK, Hadjipanayis GC. IEEE Trans Magn 1992;28:3180.
[25] Liz L, Lopez-Quintela MA, Mira J, Rivas J. J Mater Sci 1994;29:3797.
[26] Lopez-Perez JA, Lopez-Quintela MA, Mira J, Rivas J. IEEE Trans Magn 1997;33:4359.
[27] Dresco PA, Zaitsev VS, Gambino RJ, Chu B. Langmuir 1999;15:1945.
[28] Leun D, Sengupta AK. Environ Sci Technol 2000;34:3276.
[29] Shiho H, Manabe Y, Kawahashi N. J Mater Chem 2000;10:333.
[30] Sobisch T, Lerche D. Colloid Polym Sci 2000;278:369.
[31] Killmann E, Eisenlauer J. Prog Colloid Polym Sci 1976;60:147.